IEEE Photonics Journal
An IEEE Photonics Society Publication

Open Access

Data Detection and Code Channel Allocation for Frequency-Domain Spread ACO-OFDM Systems Over Indoor Diffuse Wireless Channels

Volume 6, Number 1, February 2014

Jun-Bo Wang
Peng Jiang
Jiangzhou Wang
Ming Chen
Jin-Yuan Wang

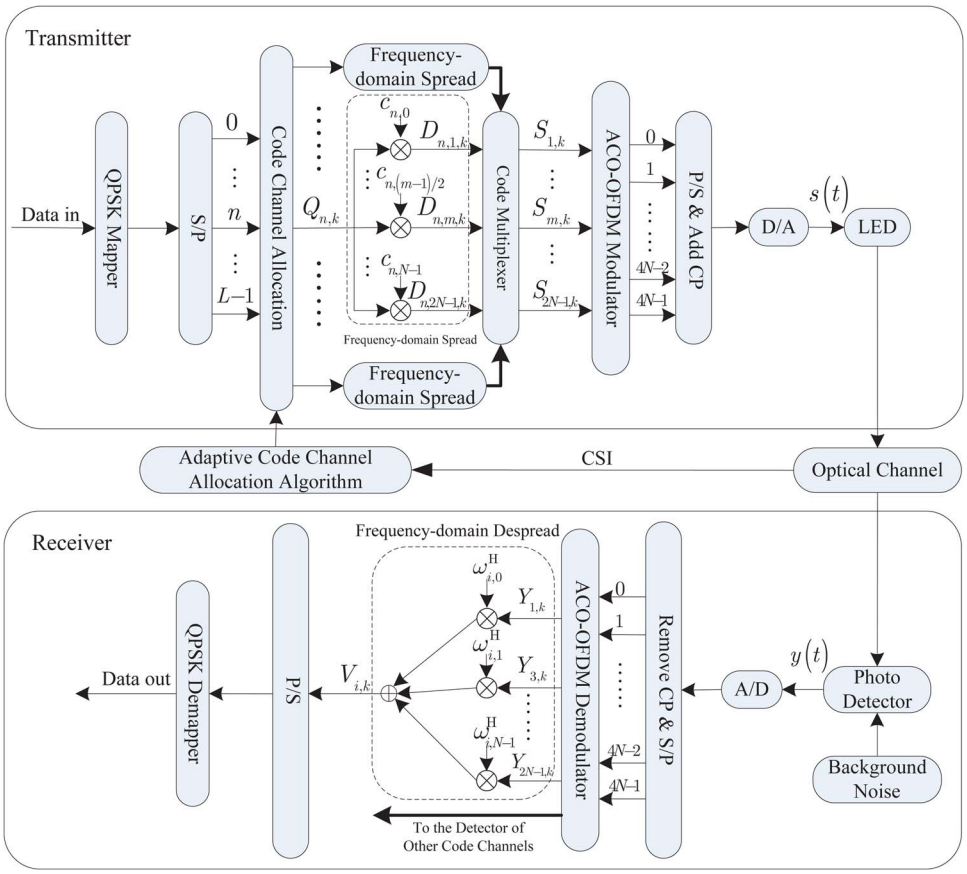

DOI: 10.1109/JPHOT.2014.2305736
1943-0655 © 2014 IEEE

Data Detection and Code Channel Allocation for Frequency-Domain Spread ACO-OFDM Systems Over Indoor Diffuse Wireless Channels

Jun-Bo Wang,[1] Peng Jiang,[2] Jiangzhou Wang,[3] Ming Chen,[1] and Jin-Yuan Wang[1]

[1]National Mobile Communications Research Laboratory, Southeast University, Nanjing 210096, China
[2]College of Electronic and Information Engineering, Nanjing University of Aeronautics and Astronautics, Nanjing 210016, China
[3]School of Engineering and Digital Arts, University of Kent, CT2 7NT Canterbury, U.K.

DOI: 10.1109/JPHOT.2014.2305736

Manuscript received January 18, 2014; revised February 2, 2014; accepted February 4, 2014. Date of publication February 12, 2014; date of current version February 21, 2014. This work was supported in part by the National Natural Science Foundation of China under Grants 61102068, 61172077, 61372106, and 61223001; by the Research Fund for the Doctoral Program of Higher Education under Grant 20113218120017; by the National 863 High Technology Development Project under Grant 2013AA01 3601; by the Key Special Project of National Science and Technology under Grant 2013ZX03003006; by the Research Fund of the National Mobile Communications Research Laboratory of Southeast University under Grants 2012D04 and 2014B01; by the Scientific Innovation Research of College Graduate in Jiangsu Province under Grant CXZZ13 0098; and by the Fundamental Research Funds for the Central Universities. Corresponding author: J.-B. Wang (e-mail: jbwang@seu.edu.cn).

Abstract: Future optical wireless communication systems promise to provide high-speed data transmission in indoor diffuse environments. This paper considers frequency-domain spread asymmetrically clipped optical orthogonal frequency-division multiplexing (ACO-OFDM) systems in indoor diffuse channels and aims to develop efficient data detection and code channel allocation schemes. By exploiting the frequency-domain spread concept, a linear multi-code detection scheme is proposed to maximize the signal to interference plus noise ratio (SINR) at the receiver. The achieved SINR and bit error ratio (BER) performance are analyzed. A computationally efficient code channel allocation algorithm is proposed to improve the BER performance of the frequency-domain spread ACO-OFDM system. Numerical results show that the frequency-domain spread ACO-OFDM system outperforms conventional ACO-OFDM systems in indoor diffuse channels. Moreover, the proposed linear multi-code detection and code channel allocation algorithm can improve the performance of optical peak-to-average power ratio (PAPR).

Index Terms: ACO-OFDM, frequency-domain spread, optical PAPR, linear multi-code detection, code channel allocation.

1. Introduction

As more and more wireless home networks are being deployed, the public industrial, scientific, and medical (ISM) unlicensed frequency band gets increasingly crowded leading to a shortage of available bandwidth, increased interference, and compromised system throughput. Meanwhile, radio frequency (RF) communications can interfere with electrical equipments, which prevents the application of RF communications in electromagnetic sensitive environments like hospitals or

aircraft cabins. Moreover, the characteristic that the RF microwave can pass through some substances, such as walls in indoor environments, also presents a security problem for secret data transmissions [1], [2]. These severe constraints associated with RF communications have motivated ones to look for other means of achieving high data rate wireless connectivity in indoor environments. Due to the benefits of the unregulated huge optical spectrum, license-free operation, immunity to electromagnetic interference, and high communication security [3], [4], optical wireless communications (OWC) has been anticipated to be an essential alternative for future low-mobility indoor wireless connections with high throughput [5]. Meanwhile, with the widespread deployment of light-emitting diodes (LEDs) for energy conservation in general lighting, OWC has attracted much attention in recent years.

Although OWC owns the unregulated huge optical spectrum, the optical devices to make full use of the whole optical spectrum are still immature and expensive. Only a small fraction of spectrum and low cost devices can be used for OWC. Moreover, the indoor OWC environment is a confined environment. The optical transmitted signals travel via multiple paths and arrive at the receiver at different time instants [6]. Experimental results have shown that the multipath propagation may cause inter-symbol interference (ISI), which will degrade the OWC system performance significantly [7]. Over the past few years, many advanced techniques have been proposed for high speed transmissions of OWC. For example, [8] proposed a spread spectrum technique to combat ISI but at the expense of reduced spectral efficiency. [9] presented the design for multiple transmitter beams and narrow multi-beam field of view (FOV) receiver to overcome multipath dispersion. In [10], guard slots and nonlinear equalizer were introduced to mitigate multipath effect. In [11], an adaptive decision equalizer with least mean square (LMS) algorithm was exploited to combat ISI. However, it should be noted that the complexity of equalization in traditional single carrier transmission schemes increases rapidly with the data rates, which motivates the necessity of the research in optical multi-carrier transmission techniques. Using the orthogonal frequency-division multiplexing technique (OFDM) [12], [13], several types of optical multi-carrier transmission techniques have been proposed to support high data rates transmission, such as direct-current-biased optical OFDM (DCO-OFDM) [14] and asymmetrically clipped optical OFDM (ACO-OFDM) [15]. However, the major drawback of optical OFDM transmission techniques is an increased peak-to-average power ratio (PAPR) yielding an increased signal dynamic range [16]. In [17], it has been shown that combining OFDM and code-division multiple access (CDMA) can offer significant reduction in the PAPR and dynamic range. This is due to the fact that all carriers in frequency-domain spread optical OFDM systems convey the same information stream and they can be adequately manipulated to obtain reduced PAPR. In [18], frequency-domain spread optical OFDM has been proved to improve the performance of OWC. However, the orthogonality among all code channels cannot be maintained due to the different gains among subcarriers [19]. Hence, the inter-channel interference (ICI) occurs and degrades the transmission performance. To the best of our knowledge, data detection and code allocation have not been studied so far to mitigate ICI in the frequency-domain spread optical OFDM.

Although ACO-OFDM retains all of the attractive properties of wireless OFDM systems, it suffers from large PAPR. In order to reduce the large PAPR in the ACO-OFDM, this paper proposes frequency-domain spread ACO-OFDM and aims to develop key techniques, such as efficient data detection and code channel allocation schemes. The main contributions of this paper are summarized as follows:

1 Formulation of effective linear multi-code detection in frequency-domain spread ACO-OFDM. Exploiting the spread concept, the optimal frequency-domain weight of multi-code detection is derived to maximize the signal to interference plus noise ratio (SINR). Moreover, the achieved SINR and bit error ratio (BER) performances are analyzed.
2 Computationally efficient algorithm to solve code channel allocation problem. The code channel allocation problem is considered as a combination optimization problem to minimize the average BER. From the implementation point of view, a computationally efficient code channel allocation algorithm is proposed.

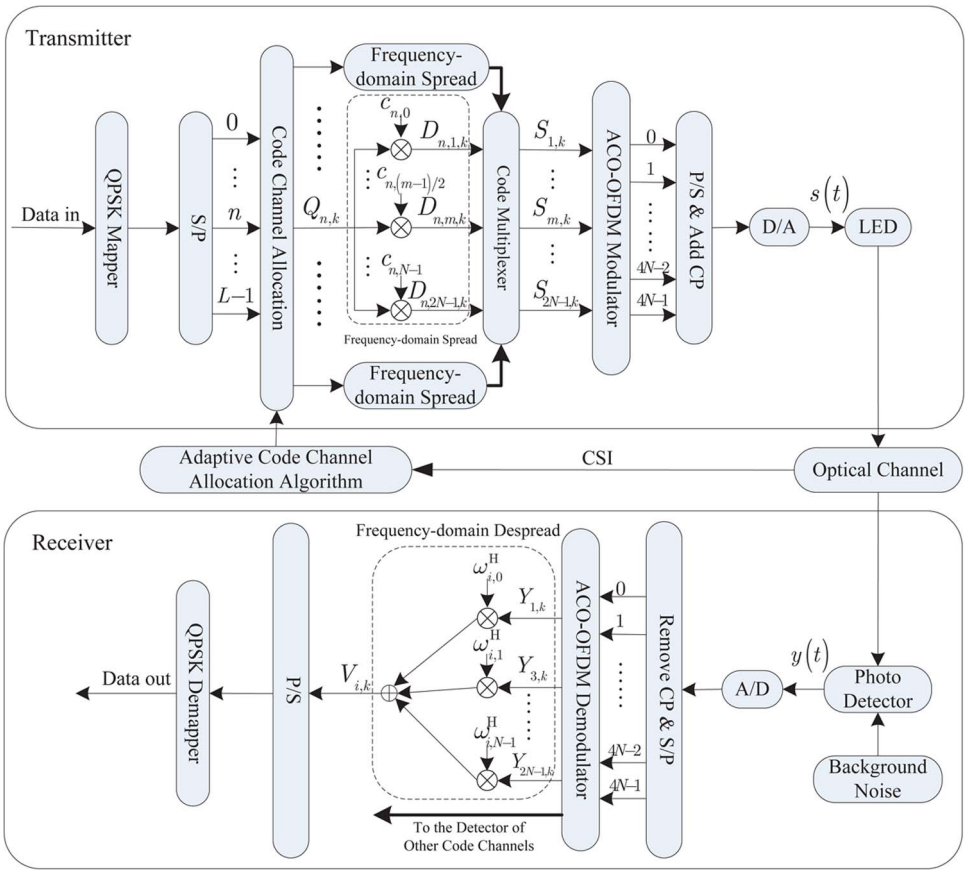

Fig. 1. Frequency-domain spread ACO-OFDM systems structure.

The remainder of this paper is organized as follows. In Section 2, the proposed frequency-domain spread ACO-OFDM system model is described. Linear multi-code detection is presented in Section 3. Adaptive code channel allocation is presented in Section 4. Numerical results are presented in Section 5. Finally, Section 6 concludes the paper.

2. System Model

2.1. Transmitter Model

The basic structure of the frequency-domain spread ACO-OFDM system is illustrated in Fig. 1. At the transmitter, 0- or 1-valued information bits are firstly mapped into quadrature phase shift keying (QPSK) symbols with Gray coding. The mapped QPSK symbols are then converted to L parallel symbol streams. Then, according to the instantaneous channel state information (CSI), the adaptive channel allocation algorithm will assign each symbol streams to a code channel. Note that each code channel is allocated with a unique orthogonal variable spreading factor (OVSF) spreading code. In this paper, the allocated OVSF spreading code of the nth $(n \in \{0, 1, \ldots, N-1\})$ code channel is denoted as $\mathbf{C}_n = \{c_{n,0}, c_{n,1}, \ldots, c_{n,N-1}\}$, where N is the code length and all code chips take "1" or "-1". The generation and some attributes of OVSF codes can be found in [20]. On each code channel, each symbol will be spread with the allocated spreading code. Then, spread symbols are combined at the code multiplexer. For instance, $N = 4$ and $E_s = 1$ are considered as an example shown in Fig. 2. An input bit sequence of {0 1 1 0} is mapped to two QPSK symbols as "$-\sqrt{2}/2 - \sqrt{2}/2\ i$" and "$\sqrt{2}/2 + \sqrt{2}/2\ i$", respectively. Then, the two symbols are spread by the

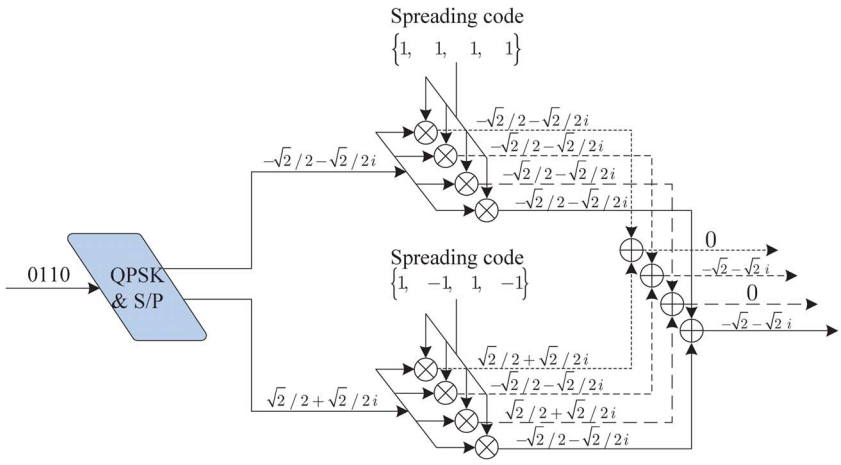

Fig. 2. Example for frequency-domain spreading and code multiplexer.

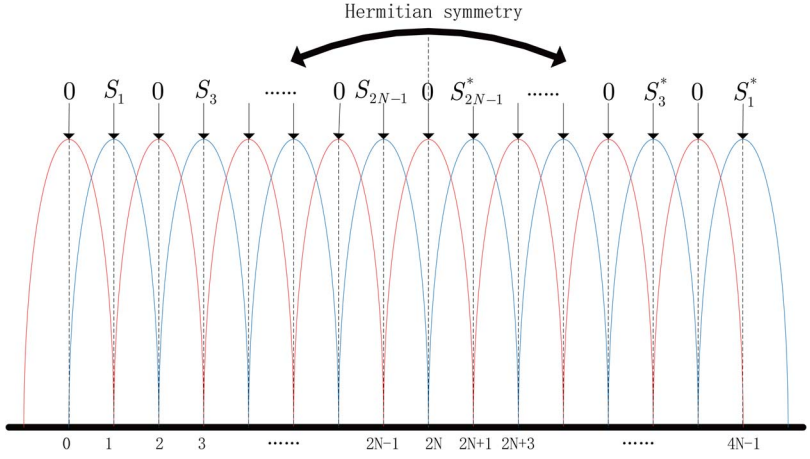

Fig. 3. Spectrum of ACO-OFDM signal.

allocated spreading codes {1, 1, 1, 1} and {1, −1, 1, −1}, respectively. Accordingly, the output of the code multiplexer is $\{0, -\sqrt{2} - \sqrt{2}\,i, 0, -\sqrt{2} - \sqrt{2}i\}$. After code multiplexing, the combined signal will be modulated to the corresponding sub-carriers by using ACO-OFDM techniques. In the ACO-OFDM, all subcarriers have Hermitian symmetry to ensure a real signal. Moreover, in order to obtain a positive signal, only the odd subcarriers are modulated by the data, as shown in Fig. 3. Obviously, the number of independent data to be transmitted in one ACO-OFDM symbol is at most 1/4 of the number of subcarriers in the ACO-OFDM [16]. Since the code length of each code channel is N, $4N$ subcarriers are required to transmit the spread data and the negative portion of symbols through the inverse discrete Fourier transform (IFFT) is simply clipped to zero. After the parallel-to-serial (P/S) operation, a cyclic prefix (CP) is appended to the unipolar signal to mitigate multi-path effect. Then, the resulting serial unipolar signal is converted to an analog signal through the digital-to-analog converter (D/A) and transmitted by modulating the optical intensity of an LED. The transmitted signal $s(t)$ is expressed as

$$s(t) = \left[\frac{1}{\sqrt{4N}} \sum_{m=0}^{4N-1} S_{m,k} \exp\left(\frac{j2\pi m(t-(k-1)T_s)}{T}\right)\right]^{+} \quad t \geq 0 \tag{1}$$

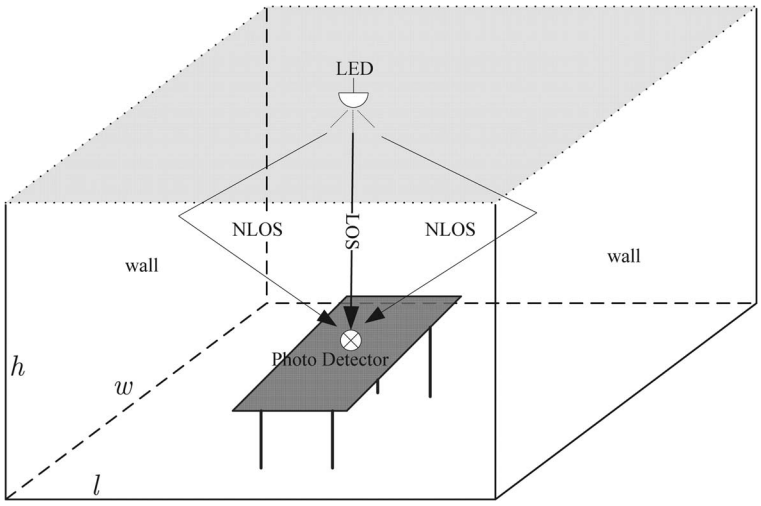

Fig. 4. Indoor optical propagation model.

where the operator $[X]^+$ is given by

$$[X]^+ = \begin{cases} X, & X \geq 0, \\ 0 & X < 0. \end{cases} \tag{2}$$

In (1), T is the period of one frequency-domain spread ACO-OFDM symbol excluding CP, T_s is the period of one frequency-domain spread ACO-OFDM symbol including CP, $S_{m,k}$ is the signal of the kth frequency-domain spread ACO-OFDM symbol on the mth subcarrier and is given by

$$S_{m,k} = \sum_{n \in \Psi} \sqrt{\frac{2E_s}{N}} D_{n,m,k} \tag{3}$$

where E_s is the transmitted electrical power per symbol of one code channel, the coefficient "2" accounts for the compensation of the total electrical power loss due to the clipping operation, $\Psi \subseteq \{0, 1, \ldots, N-1\}$ is the set of allocated code channels, $D_{n,m,k}$ is the replica of the kth frequency-domain spread ACO-OFDM symbol of nth code channel on the mth subcarrier, expressed as

$$D_{n,m,k} = \begin{cases} c_{n,(m-1)/2} Q_{n,k}, & m = 1, 3, \ldots, 2N-1 \\ 0, & m = 0, 2, \ldots, 2N-2, \\ (D_{n,4N-m,k})^*, & 2N \leq m \leq 4N-1 \end{cases} \tag{4}$$

where $Q_{n,k}$ is the mapped data symbol with unit power of the kth frequency-domain spread ACO-OFDM symbol of the nth code channel.

2.2. Channel Model

Consider a indoor scenario shown in Fig. 4, the optical wireless channel is generated by the analytical model developed in [21]. The model includes both line of sight (LOS) component and diffuse components. The time-domain impulse response is given by [21]

$$h(t) = \eta_{\text{LOS}} \delta(t) + h_{\text{diff}}(t - \Delta T) \tag{5}$$

where η_{LOS} is the gain of LOS signal, $\delta(t)$ is the Dirac function, and ΔT represents the delay of the first arriving diffuse signal relative to the LOS component. The frequency-domain response of (5) is given by [21]

$$H(f) = \eta_{\text{LOS}} + H_{\text{diff}}(f) \tag{6}$$

where the diffuse component has a low pass characteristic given by [21]

$$H_{\text{diff}}(f) = \eta_{\text{diff}} \frac{e^{j2\pi f \Delta T}}{1 + j\frac{f}{f_0}} \tag{7}$$

where η_{diff} is the gain of diffuse signal, and f_0 is the cutoff frequency. In this room, the surface area is S_{room}, the volume is V_{room}, and the reflectivity of the surfaces is ρ. Then η_{diff} and f_0 can be calculated as [21]

$$\eta_{\text{diff}} = \frac{S_{\text{RX}}}{S_{\text{room}}} \cdot \frac{\rho}{1-\rho} \tag{8}$$

$$f_0 = -\frac{\text{c} \cdot \ln\rho}{8\pi} \cdot \frac{S_{\text{room}}}{V_{\text{room}}} \tag{9}$$

where S_{RX} represents the effective receiver area and c represents the light speed. Moreover, a K-factor is defined to describe the electrical power ratio of LOS component to diffuse component and given by [21]

$$K = 20\log\frac{\eta_{\text{LOS}}}{\eta_{\text{diff}}}. \tag{10}$$

2.3. Receiver Model

At the receiver, the photo detector (PD) transforms the received optical intensity into electrical signal. The detected electrical signal plus noise is expressed as

$$y(t) = s(t) \otimes h(t) + z(t) \tag{11}$$

where "$\otimes$" means the convolution operator, $h(t)$ is the impulse response of the optical channel, $z(t)$ stands for both thermal noise and ambient-light-induced shot noise. Here, the noise is modeled as a Gaussian random variable [22]. The analog signal $y(t)$ is converted back to digital through the analog-to-digital converter (A/D). After removing CP and the serial-to-parallel (S/P) operation, the resulting signal will be sent to the ACO demodulator. Then, the kth received frequency domain signal on the mth subcarrier is given by

$$Y_{m,k} = \frac{1}{2}\sum_{n\in\Psi}\sqrt{\frac{2E_s}{N}} D_{n,m,k} \cdot H_m + Z_{m,k}, \quad m = 1, 3, \ldots, 4N-1 \tag{12}$$

where the coefficient "1/2" accounts for the effect of the clipping, H_m is the gain on the mth subcarrier between the input to the optical modulator in the transmitter and the output of the optical detector in the receiver, and $Z_{m,k}$ is the background noise at the receiver. Since the data is transmitted only on the odd subcarriers, the outputs on the even subcarriers are discarded after the demodulation of ACO-OFDM. Considering the Hermitian symmetry shown in (4), only the first half odd subcarrier data is used in the detection. Thus, the demodulated signal of the kth frequency-domain spread-ACO-OFDM symbol can be expressed in the matrix form as

$$\mathbf{Y}_k = \sqrt{\frac{E_s}{2N}}\sum_{n\in\Psi}\text{diag}(\mathbf{C}_n)\mathbf{H}Q_{n,k} + \mathbf{Z}_k \tag{13}$$

where $\mathbf{Y}_k = [Y_{1,k}, Y_{3,k}, \ldots, Y_{2N-1,k}]^{\text{T}}$, $\mathbf{H} = [H_1, H_3, \ldots, H_{2N-1}]^{\text{T}}$, $\mathbf{Z}_k = [Z_{1,k}, Z_{3,k}, \ldots, Z_{2N-1,k}]^{\text{T}}$ stand for the vectors of received signals, optical channel frequency gains, and background noises, respectively. Then, the demodulated signals are further multiplied by the frequency-domain combining weights and combined at the frequency domain despreader to get the decision variable for the desired channel. The resultant decision variable will be parallel-to-serial (P/S) converted and put into the QPSK demapper. Finally, the transmitted information bits on the desired channel are obtained.

3. Linear Multi-Code Detection

In ideal Gaussian channels, all code channels of frequency-domain spread ACO-OFDM are orthogonal in frequency-domain. However, in realistic indoor diffuse channels, the orthogonality among code channels no longer maintains due to the frequency selectivity. Moreover, severe ICI will occur in non-orthogonal code channels. In order to improve performance, the ICI must be minimized as much as possible. This section tries to mitigate the effects of ICI by proposing advanced data detection technique.

In traditional CDMA systems, data detection can usually be classified as single-code (single-user) detection or multi-code (multi-user) detection. The approach using single-code detection aims to compensate for the distortion due to fading on each sub-channel, but not taking into account any information about the ICI. Meanwhile, multi-code detection uses the spread structure to minimize the effects of ICI. Multi-code detection outperforms single-code detection [23]. In this paper, a linear multi-code detection scheme is proposed for the frequency-domain spread ACO-OFDM systems. Since a higher received SINR will lead to a lower error probability of data detection, we consider to maximize the received SINR by selecting the frequency-domain weight of multi-code detection.

Assuming the frequency-domain weight for the ith code channel is $\mathbf{w}_i = [w_{i,0}, w_{i,1}, \ldots, w_{i,N-1}]^{\mathrm{T}}$, the decision variable of the kth frequency-domain spread-ACO-OFDM symbol of the ith code channel can be obtained as

$$V_{i,k} = \mathbf{w}_i^{\mathrm{H}} \mathbf{Y}_k, \quad i \in \Psi \tag{14}$$

where $(\cdot)^{\mathrm{H}}$ stands for conjugate transposition. Substituting $\mathbf{Y}_k$ in (14) with (13), $V_{i,k}$ is given by

$$V_{i,k} = \mathbf{w}_i^{\mathrm{H}} \sqrt{\frac{E_s}{2N}} \mathrm{diag}(\mathbf{C}_i)\mathbf{H}Q_{i,k} + \mathbf{w}_i^{\mathrm{H}} \sqrt{\frac{E_s}{2N}} \sum_{n \neq i, n \in \Psi} \mathrm{diag}(\mathbf{C}_n)\mathbf{H}Q_{n,k} + \mathbf{w}_i^{\mathrm{H}} \mathbf{Z}_k. \tag{15}$$

It should be noted that the first term on the right-hand side of (15) is the desired signal, the second one is the ICI from other code channels, and the third term is the noise term. From (15), the instantaneous received SINR of ith code channel can be derived as

$$\begin{aligned} \gamma_i &= \frac{\mathrm{E}_{Q_{i,k}} \left\{ \left| \mathbf{w}_i^{\mathrm{H}} \sqrt{\frac{E_s}{2N}} \mathrm{diag}(\mathbf{C}_i)\mathbf{H}Q_{i,k} \right|^2 \right\}}{\mathrm{E}_{Q_{n,k}, \mathbf{Z}_k} \left\{ \left| \mathbf{w}_i^{\mathrm{H}} \sqrt{\frac{E_s}{2N}} \sum_{n \neq i, n \in \Psi} \mathrm{diag}(\mathbf{C}_n)\mathbf{H}Q_{n,k} + \mathbf{w}_i^{\mathrm{H}} \mathbf{Z}_k \right|^2 \right\}} \\ &= \frac{\frac{E_s}{2N} \mathbf{w}_i^{\mathrm{H}} \mathrm{diag}(\mathbf{C}_i)\mathbf{H}(\mathrm{diag}(\mathbf{C}_i)\mathbf{H})^{\mathrm{H}} \mathbf{w}_i}{\mathbf{w}_i^{\mathrm{H}} \left(\frac{E_s}{2N} \left(\sum_{n \neq i, n \in \Psi} (\mathrm{diag}(\mathbf{C}_n)\mathbf{H})(\mathrm{diag}(\mathbf{C}_n)\mathbf{H})^{H} \right) + \sigma^2 I_N \right) \mathbf{w}_i} \\ &= \frac{\frac{E_s}{2N} \mathbf{w}_i^{\mathrm{H}} \mathrm{diag}(\mathbf{C}_i)\mathbf{H}(\mathrm{diag}(\mathbf{C}_i)\mathbf{H})^{\mathrm{H}} \mathbf{w}_i}{\mathbf{w}_i^{\mathrm{H}} (\mathbf{R}_i) \mathbf{w}_i} \end{aligned} \tag{16}$$

where $\mathrm{E}_X\{\}$ denotes the expectation with respect to X, σ^2 is the variance of the background noise, I_N is $N \times N$ identity matrix, $\mathbf{R}_i$ is a positive definite Hermitian matrix, given by

$$\mathbf{R}_i = \frac{E_s}{2N} \left(\sum_{n \neq i, n \in \Psi} (\mathrm{diag}(\mathbf{C}_n)\mathbf{H})(\mathrm{diag}(\mathbf{C}_n)\mathbf{H})^{\mathrm{H}} \right) + \sigma^2 I_N. \tag{17}$$

Using the property of positive definite Hermitian matrix, (17) can be expressed as

$$\mathbf{R}_i = \mathbf{L}\mathbf{L}^{\mathrm{H}} \tag{18}$$

where $\mathbf{L} \in \mathbb{C}^{N\times N}$ is an invertible matrix. To facilitate the following derivation, let $\tilde{\mathbf{w}}_i = \mathbf{L}^{\mathrm{H}}\mathbf{w}_i$ and $\tilde{\mathbf{a}}_i = \mathbf{L}^{-1}\mathrm{diag}(\mathbf{C}_i)\mathbf{H}$. Then (16) can be further rewritten as:

$$\gamma_i = \frac{E_s}{2N}\frac{\tilde{\mathbf{w}}_i^{\mathrm{H}}\tilde{\mathbf{a}}_i\tilde{\mathbf{a}}_i^{\mathrm{H}}\tilde{\mathbf{w}}_i}{\tilde{\mathbf{w}}_i^{\mathrm{H}}\tilde{\mathbf{w}}_i}. \tag{19}$$

Therefore, the optimal $\tilde{\mathbf{w}}_i$ to maximize γ_i can be obtained by solving the following problem:

$$\max_{\tilde{\mathbf{w}}_i\in\mathbb{C}^{n\times 1}} \frac{\tilde{\mathbf{w}}_i^{\mathrm{H}}\tilde{\mathbf{a}}_i\tilde{\mathbf{a}}_i^{\mathrm{H}}\tilde{\mathbf{w}}_i}{\tilde{\mathbf{w}}_i^{\mathrm{H}}\tilde{\mathbf{w}}_i}. \tag{20}$$

Note that $\tilde{\mathbf{a}}_i\tilde{\mathbf{a}}_i^{\mathrm{H}}$ is a Hermitian matrix. According to the Rayleigh-Ritz Theorem in [24, Sec. 4.2], it can be known that the maximum value of the objective in (20) is bounded by the maximum eigenvalue of $\tilde{\mathbf{a}}_i\tilde{\mathbf{a}}_i^{\mathrm{H}}$. Moreover, the optimal $\tilde{\mathbf{w}}_i$ to maximize γ_i is $\tilde{\mathbf{a}}_i$. By carrying out matrix operations, the optimal frequency weight $\mathbf{w}_i$ of multi-code detector is derived as

$$\mathbf{w}_i = (\mathbf{R}_i)^{-1}(\mathrm{diag}(\mathbf{C}_i)\mathbf{H}). \tag{21}$$

Substituting $\mathbf{w}_i$ in (16) with (21), the maximum value of received SINR can be obtained as

$$\gamma_i^{\max} = \frac{E_s}{2N}(\mathrm{diag}(\mathbf{C}_i)\mathbf{H})^{\mathrm{H}}(\mathbf{R}_i)^{-1}(\mathrm{diag}(\mathbf{C}_i)\mathbf{H}). \tag{22}$$

It is shown from the central limit theorem in [25, Sec. 2.5] that the sum of a sufficiently large number of independent random variables can be approximated as normal distribution. Therefore, the ICI in frequency-domain spread ACO-OFDM systems tends toward a Gaussian distribution. From the symbol error rate expression [26, Eq. (9.25)], the BER performance of the ith code channel can be estimated as

$$\mathrm{BER}_i = Q\left(\sqrt{\gamma_i^{\max}}\right) \tag{23}$$

where $Q(x) = (1/2\pi)\int_x^{\infty}\exp(-(u^2/2))\mathrm{du}$.

4. Adaptive Code Channel Allocation

Along with the loss of orthogonality among all code channels in indoor diffused channels, the cross-correlation properties among code channels are not zero due to different gains among subcarriers. Moreover, for every two code channels, the code channel correlations may not be the same, which also results in the ICI differences among different combinations of code channels. Therefore, the ICI between every two code channels may not be the same. Since the level of ICI is dependent on which code channels to be used [27], this section is to minimize the ICI by allocating an appropriate combination of code channels.

From (22), when only one code channel is allocated to transmit data, i.e., $L = 1$, there is no ICI for the data detection. In this case, if the ith code channel is allocated for transmission, the maximum received SINR of the ith code channel is simplified as

$$\gamma_i^{\max} = \frac{E_s}{2N\cdot\sigma^2}\sum_{j=0}^{N-1}|H_{2j+1}|^2. \tag{24}$$

In the case of $L = 1$, any code channel can be allocated for data transmission and get the same transmission performance. Further, if all the available code channels are allocated to transmit data, i.e., $L = N$, a closed-form expression can be derived for the received SINR as

$$\gamma_i^{\max} = \frac{\dfrac{E_s}{2N}\displaystyle\sum_{j=0}^{N-1}\frac{|H_{2j+1}|^2}{\frac{1}{2}E_s|H_{2j+1}|^2+\sigma^2}}{1-\dfrac{E_s}{2N}\displaystyle\sum_{j=0}^{N-1}\frac{|H_{2j+1}|^2}{\frac{1}{2}E_s|H_{2j+1}|^2+\sigma^2}}, \quad i = 0, 1, \ldots, N-1. \tag{25}$$

TABLE 1

The proposed code channel allocation algorithm.

Step 1 If $L = 1$,
output $\Psi = \{0\}$, i.e. allocate the 0th code channel to transmit data;
else go to Step 2;
Step 2 If $L = N$,
output $\Psi = \{0, 1, \cdots, N-1\}$, i.e. allocate all code channels to transmit data;
else go to Step 3;
Step 3 Initialization. $\Psi = \{0\}$, $\bar{\Psi} = \{1, \cdots, N-1\}$;
Step 4 while $|\Psi| < L$ do
a) Find the code channel satisfying

$$\varepsilon = \arg\min_{\tau \in \bar{\Psi}} P(\Psi \cup \{\tau\}) \tag{28}$$

b) $\Psi = \Psi \cup \{\varepsilon\}$, $\bar{\Psi} = \bar{\Psi} \backslash \{\varepsilon\}$;
Step 5 Output Ψ.

(25) indicates that all code channels own the same transmission performance when the system is full load. However, for $1 < L < N$, it is necessary to investigate how to allocate code channels to minimize the effects of ICI and improve system BER performance.

As Ψ is the set of allocated code channels, the system BER performance can be calculated as

$$P(\Psi) = \frac{1}{L} \sum_{i \in \Psi} \mathrm{BER}_i. \tag{26}$$

Accordingly, the code channel allocation problem can be formulated as the following optimization problem:

$$\min_{\Psi \subseteq \{0,1,\ldots,N-1\}} P(\Psi)$$
$$\text{s.t.}$$
$$|\Psi| = L \tag{27}$$

where $|\Psi|$ denotes the element number of the set Ψ and L is the number of allocated code channels.

In the optimization problem (27), there exist $N!/(K!(N-K)!)$ possible code channel allocations. The minimum value of the objective function over all $N!/(K!(N-K)!)$ allocations is globally minimum, and the corresponding code channel allocation is the optimal solution. However, the optimization problem (27) is a combination optimization problem, which has been proven to be a nondetermined-polynomial-time complete problem without computationally efficient algorithms to obtain the optimal solution. However, from the implementation point of view, computationally efficient algorithms are more preferred. Therefore, a computationally efficient code channel allocation algorithm is proposed in Table 1.

5. Numerical Results

This section will evaluate the frequency-domain spread ACO-OFDM system in terms of optical PAPR performance at the transmitter and BER performance at the receiver. The performance of ACO-OFDM is also shown for comparison. In this paper, the optical PAPR is defined as the ratio between the maximum optical power and the average optical power of a transmitted signal, that is

$$\text{optical PAPR}(s(t)) \triangleq \frac{\max\{s(t)\}}{\mathrm{E}\{s(t)\}} \tag{29}$$

where $\max\{X\}$ stands for the maximum value of X. It is meaningless to determine the exact value of optical PAPR since the optical PAPR of a transmitted signal is a random variable. Usually, the

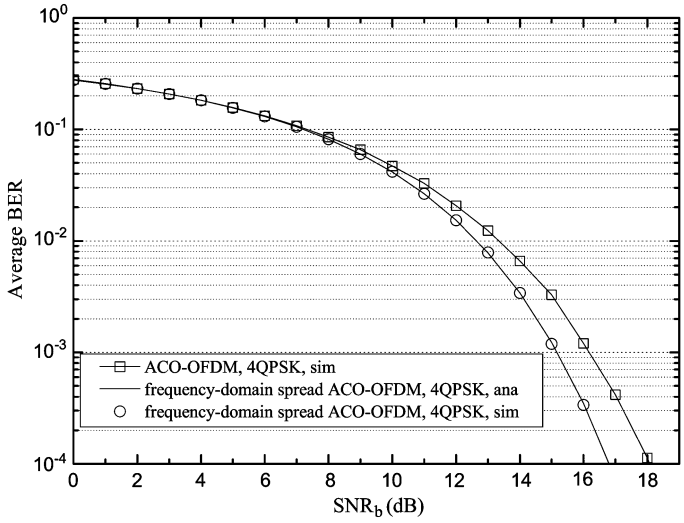

Fig. 5. BER performance of frequency-domain spread ACO-OFDM and ACO-OFDM.

complementary cumulative distribution function (CCDF), denoting the probability exceeding a certain optical PAPR threshold η, is used to indicate the optical PAPR performance and given by

$$\text{CCDF} = \Pr\{\text{optical} \quad \text{PAPR}(s(t)) > \eta\}. \tag{30}$$

In order to evaluate the BER performance, we consider a room with length and width of 5 meters, height of 3 meters, average reflectivity of all of the surfaces of 0.6, and the effective receiver area is set to 16 mm^2. Meanwhile, code length is set to be $N = 16$. According to the structure of ACO-OFDM, at most, N independent data steams can be transmitted on $4N$ subcarriers. Therefore, the number of subcarriers is set to be 64 and the number of cyclic prefix is set to be $N_{cp} = 16$. To facilitate the following description, the transmit power is measured by the average SNR per bit, defined as $\text{SNR}_b = E_s/(2\sigma^2)$.

In this section, the results are organized as follows. First, the performance of frequency-domain spreading with linear multi-code detection is presented. Secondly, the performance of adaptive channel allocation is presented. Finally, the effect of PAPR reduction on the BER performance is shown. According to these representative results, useful conclusions are drawn in the last section correspondingly.

5.1. Performance of Frequency-Domain Spreading With Linear Multi-Code Detection

Fig. 5 shows the BER performance as a function of the SNR_b. The frequency-domain spread ACO-OFDM symbol period T, the time delay ΔT, and the K-factor are set to be 800 ns, 10 ns, and 0 dB, respectively. For comparison, all available subcarriers in ACO-OFDM and all available code channels in the frequency-domain spread ACO-OFDM have been used for transmission. Accordingly, the two systems have the same transmission rate. It can be seen from Fig. 5 that BER performances of ACO-OFDM and frequency-domain spread ACO-OFDM systems improve with the increase of SNR_b. Moreover, when SNR_b is high, the BER performance of the frequency-domain spread ACO-OFDM system with the proposed linear multi-code detection outperforms that of ACO-OFDM system significantly.

Fig. 6 shows the optical PAPR performance of the frequency-domain spread ACO-OFDM and ACO-OFDM signals. It can be seen from Fig. 6 that that when optical PAPR threshold is beyond 6 dB, the CCDF curve of the frequency-domain spread ACO-OFDM is below that of ACO-OFDM, which means that the optical PAPR performance of the frequency-domain spread ACO-OFDM outperforms that of ACO-OFDM. In particular, at $\text{CCDF} = 10^{-2}$, the optical PAPR threshold values of ACO-OFDM and frequency-domain spread ACO-OFDM are 9.9 dB and 9.0 dB, respectively. In other

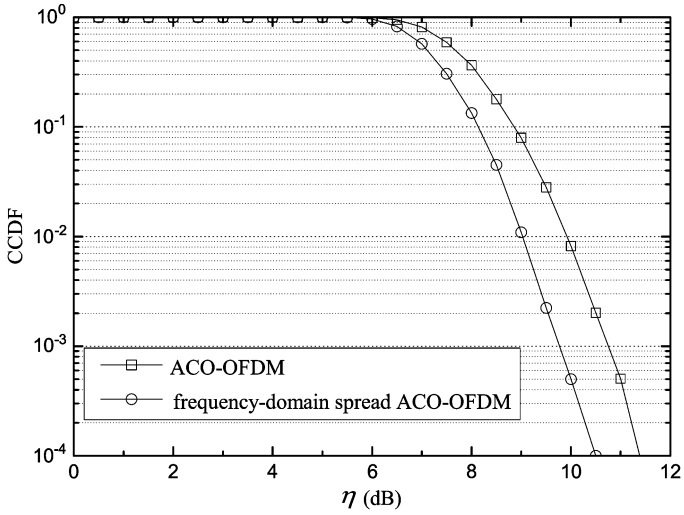

Fig. 6. CCDF of optical PAPR of frequency-domain spread ACO-OFDM signal and ACO-OFDM signal.

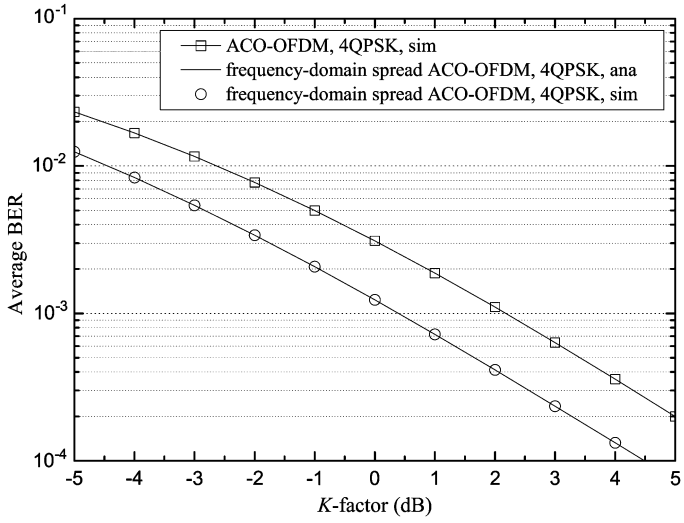

Fig. 7. BER performance as a function of K-factor.

words, the frequency-domain spreading operation improves the optical PAPR performance about 9%. This is because the frequency-domain spread can decrease the probability of the high peaks by reducing the autocorrelation of the input sequence before IFFT.

Fig. 7 shows the BER performance as a function of K-factor. SNR_b is set to be 15 dB and the frequency-domain spread ACO-OFDM symbol period T is set to be 800 ns. Note that increasing K-factor in the optical wireless channel model will increase the LOS component and reduce the multipath effects. Therefore, it can be seen that the BER performances improve with the increase of K-factor. Moreover, regardless of the K-factor, the frequency-domain spread ACO-OFDM system with the proposed linear multi-code detection outperforms the ACO-OFDM system significantly.

Fig. 8 shows the BER performance as a function of the frequency-domain spread ACO-OFDM symbol period. SNR_b is set to be 15 dB and the K-factor is 0 dB. Since the high speed transmissions, with shorter symbol period T, are prone to be affected by the multi-path effects, the ICI increases with the decrease of the symbol period T. Therefore, it can be seen that the BER performances improve with the increase of the symbol period T. Moreover, regardless of the symbol period T, the

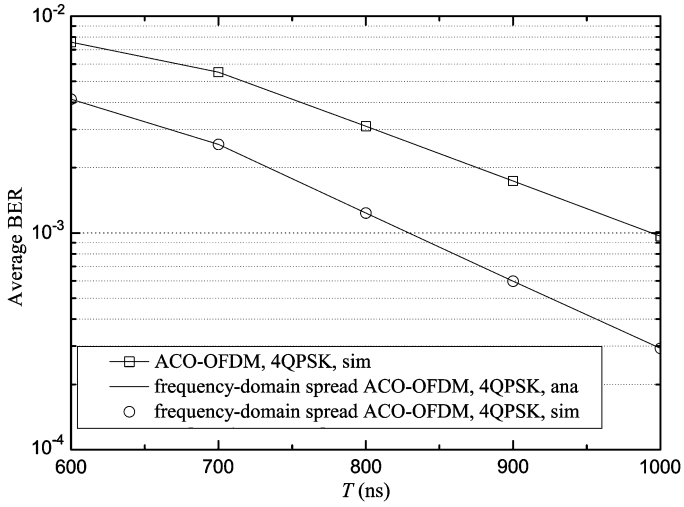

Fig. 8. BER performance as a function of T.

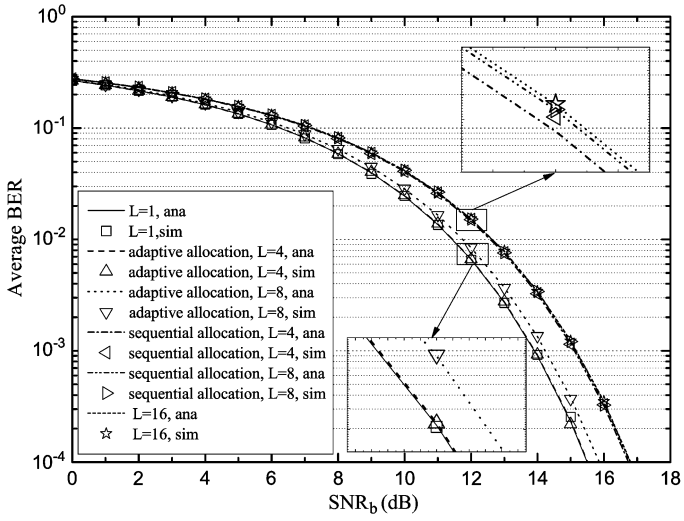

Fig. 9. BER performance of multiple code channels with adaptive allocation and sequential allocation.

frequency-domain spread ACO-OFDM system with the proposed linear multi-code detection outperforms ACO-OFDM system significantly.

5.2. Performance of Adaptive Channel Allocation

Fig. 9 shows the effects of adaptive code channel allocation on the BER performance of the frequency-domain spread ACO-OFDM system. The frequency-domain spread ACO-OFDM symbol period T, the time delay ΔT, and the K-factor are set to be 800 ns, 10 ns, and 0 dB, respectively. The sequential code channel allocation scheme is adopted for comparison. For the sequential code channel allocation, the code channels are simply allocated sequentially according to their index. More specifically, if L code channels are required, the set of allocated code channels can be described as $\Psi = \{0, 1, \ldots, L-1\}$. It can be seen that when $L = 1$ or $L = N$, both the adaptive code channel allocation and the sequential code channel allocation have the same BER performance, as discussed in Section 4. Since increasing the number of used code channels will increase the ICI in the frequency-domain spread ACO-OFDM, the BER performances degrade with the increase of the

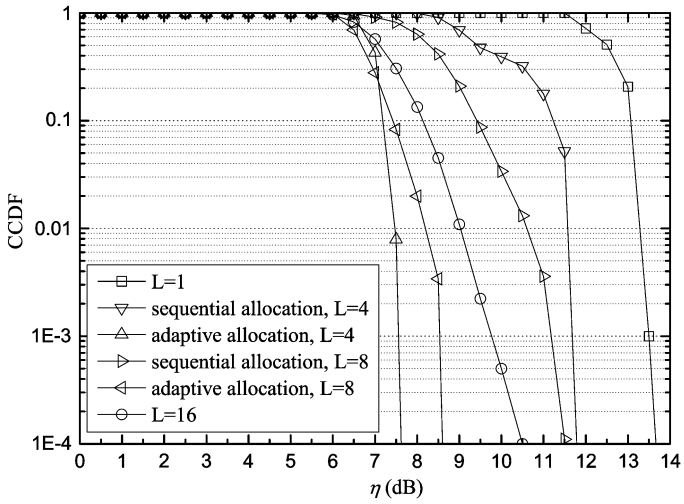

Fig. 10. CCDF of optical PAPR of frequency-domain spread ACO-OFDM signal with adaptive allocation and sequential allocation.

number of used code channels. Moreover, it can be seen that when $L = 4$ and $L = 8$, the curves of the adaptive code channel allocation are close to that of $L = 1$ and the curves of the adaptive code channel allocation are close to that of $L = 16$, which indicates that the adaptive channel allocation can reduce the ICI significantly by selecting an appropriate combination of code channels.

Fig. 10 shows the effects of adaptive code channel allocation on the optical PAPR of frequency-domain spread ACO-OFDM signal. From Fig. 10, it can be seen that the adaptive code channel allocation coherently has better optical PAPR performance. In particular, when CCDF $= 10^{-2}$, the optical PAPR thresholds of adaptive code channel allocation are lower than that of the sequential code channel allocation about 4.2 dB for $L = 4$ and 2.4 dB for $L = 8$, respectively. In other words, the adaptive code channel allocation can improve the optical PAPR performance about 36% for $L = 4$ and 23% for $L = 8$, respectively, compared with the sequential code channel allocation. It can be explained that, in frequency-domain spread ACO-OFDM systems, the orthogonality among all code channels cannot be maintained at the receiver due to the different channel gains among subcarriers. Hence, the ICI will occur and increase with increasing correlation among code channels at the receiver. By minimizing the BER, the proposed code allocation algorithm can reduce the effects of ICI, resulting in the reduction of the correlation among the allocated code channels at the receiver. Such reduction of the code channel correlation may reduce the occurrence of the high peaks in time-domain signal. Therefore, the proposed code channel allocation can improve the optical PAPR performance of the frequency-domain spread ACO-OFDM signal significantly. It should be noted that when only one code channel is active in the system $(L = 1)$, the optical PAPR value will be equal to the optical PAPR value of the spreading code. Unfortunately, the OVSF sequences have a bad property so that most of them have high PAPR values [28]. Therefore, the CCDF curve of optical PAPR for $L = 1$ is far above other curves.

5.3. The Effect of PAPR Reduction on the BER Performance

In order to show the effect of PAPR reduction on the BER performance, the LED nonlinearity can be modeled as the clipping effect [16]

$$s_{\text{cilp}}(t) = \begin{cases} s(t), & |s(t)| \le A \\ A, & |s(t)| > A \end{cases}, \tag{31}$$

and the clipping ratio (CR) is defined as [16]

$$CR = 20\log_{10}\left(\frac{A}{\sigma_s}\right) \quad \text{dB} \tag{32}$$

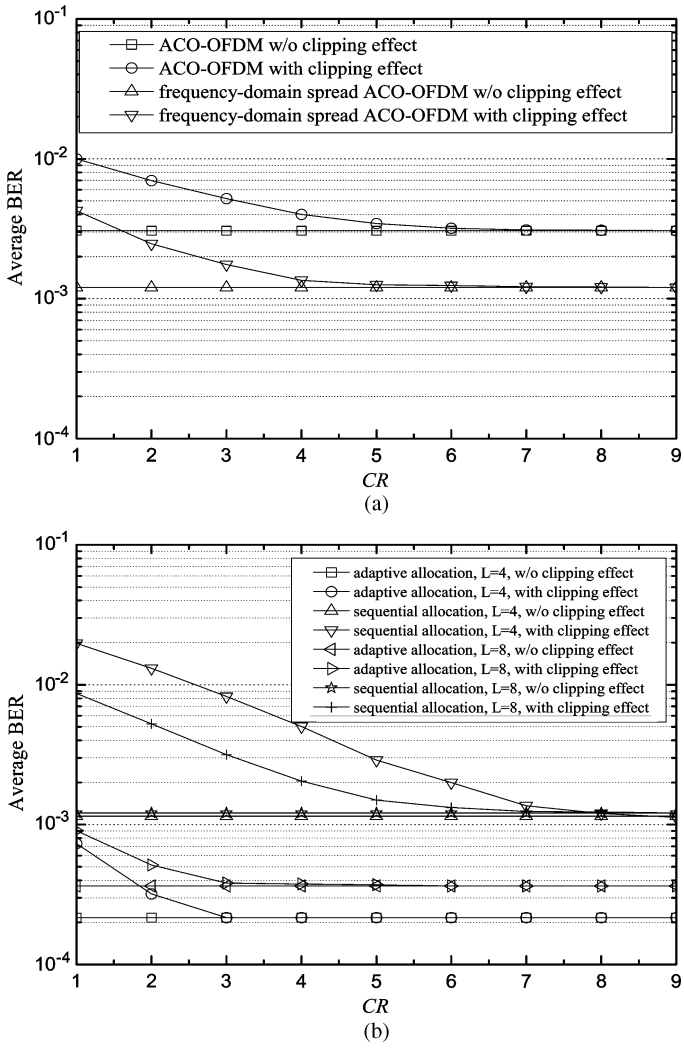

Fig. 11. The clipping effects on the BER performance. (a) The clipping effects on the BER performance of frequency-domain spread ACO-OFDM and ACO-OFDM. (b) The clipping effects on the BER performance of multiple code channels with adaptive allocation and sequential allocation.

where σ_s^2 is power of the $s(t)$, CR denotes the level of clipping effect. The larger the CR is, the more serious is the nonlinearity of LED. Fig. 11(a) and (b) show the clipping effects on BER performance. The frequency-domain spread ACO-OFDM symbol period T, the time delay ΔT, the K-factor, and $\mathrm{SNR_b}$ are set to be 800 ns, 10 ns, 0 dB, and 15 dB, respectively. It can be seen from the two figures that the BER performance degrades with decreasing CR, which indicates the LED nonlinearity is harmful for the system transmission performance. By reducing the PAPR value, the effect of LED nonlinearity can be eliminated as much as possible. More specifically, it can be seen from Fig. 11(a) that when $CR \geq 6$ dB, the clipping effect can be ignored for the ACO-OFDM. Meanwhile, the clipping effect on the frequency-domain ACO-OFDM is still very small when $CR = 5$ dB. It also can be seen from Fig. 11(b) that when $CR < 6$ dB, the clipping effects of both $L = 4$ and $L = 8$ cannot be ignored for the sequential channel allocation. However, regardless of $L = 4$ or $L = 8$, when $CR = 3$ dB, the BER degradations by the clipping effect are still very small for the adaptive channel allocation. The two figures indicate that the PAPR reduction resulting from the frequency-domain spreading and the adaptive channel allocation can reduce the clipping effect from the LED nonlinearity and improve the BER performance.

6. Conclusion

In order to reduce the large PAPR in the ACO-OFDM, this paper proposes frequency-domain spread ACO-OFDM and develops efficient data detection and adaptive code channel allocation schemes. The main conclusions are drawn as follows:

1 When the system is fully loaded, the frequency-domain spread ACO-OFDM outperforms the conventional ACO-OFDM systems in terms of optical PAPR performance. Specifically, the frequency-domain spreading operation improves the optical PAPR performance about 9% at CCDF $= 10^{-2}$.
2 When the system is not fully loaded, the proposed adaptive code channel allocation can further improve the optical PAPR performance of frequency-domain spread ACO-OFDM. At CCDF $= 10^{-2}$, the optical PAPR performance can be improved about 36% for the number of code channels $L = 4$ and 23% for $L = 8$, respectively.
3 The proposed linear multi-code detection can improve the BER performance of frequency-domain spread ACO-OFDM in indoor diffuse channels. As the K-factor (the ratio of the LOS component to diffuse component) is bigger or the symbol period T is shorter, the improvement of BER performance is more since the multipath effect is more serious.
4 The PAPR reduction resulting from the frequency-domain spreading and adaptive channel allocation can reduce the effects from the LED nonlinearity and improve the BER performance for practical systems.

References

[1] J.-B. Wang, Y. Jiao, X. Song, and M. Chen, "Optimal training sequences for indoor wireless optical communications," *J. Opt.*, vol. 14, no. 1, p. 015401, Jan. 2012.
[2] J.-B. Wang, Y. Jiao, X. Song, X. Zhao, M. Gu, M. Chen, X.-X. Xie, and M. Sheng, "Complementary sequences–based channel estimation for diffuse wireless optical communications," *Opt. Eng.*, vol. 50, no. 7, pp. 075003-1–075003-6, Jul. 2011.
[3] S. Navidpour, M. Uysal, and M. Kavehrad, "BER performance of free-space optical transmission with spatial diversity," *IEEE Trans. Wireless Commun.*, vol. 6, no. 8, pp. 2813–2819, Aug. 2007.
[4] I. Ansari, F. Yilmaz, and M.-S. Alouini, "Impact of pointing errors on the performance of mixed RF/FSO dual-hop transmission systems," *IEEE Wireless Commun. Lett.*, vol. 2, no. 3, pp. 351–354, Jun. 2013.
[5] J.-B. Wang, Q.-S. Hu, J. Wang, M. Chen, and J.-Y. Wang, "Tight bounds on channel capacity for dimmable visible light communications," *J. Lightwave Technol.*, vol. 31, no. 23, pp. 3771–3779, Dec. 2013.
[6] D.-Q. Ding and X.-Z. Ke, "A new indoor VLC channel model based on reflection," *Optoelectron. Lett.*, vol. 6, no. 4, pp. 295–298, Jul. 2010.
[7] J. Barry, J. Kahn, W. Krause, E. Lee, and D. Messerschmitt, "Simulation of multipath impulse response for indoor wireless optical channels," *IEEE J. Sel. Areas Commun.*, vol. 11, no. 3, pp. 367–379, Apr. 1993.
[8] K. K. Wong, T. O'Farrell, and M. Kiatweerasakul, "Infrared wireless communication using spread spectrum techniques," *Proc. Inst. Elect. Eng.—Optoelectron.*, vol. 147, no. 4, pp. 308–314, Aug. 2000.
[9] J. Carruther and J. Kahn, "Angle diversity for nondirected wireless infrared communication," *IEEE Trans. Commun.*, vol. 48, no. 6, pp. 960–969, Jun. 2000.
[10] Z. Ghassemlooy, A. Hayes, and B. Wilson, "Reducing the effects of intersymbol interference in diffuse DPIM optical wireless communications," *Proc. Inst. Elect. Eng.—Optoelectron.*, vol. 150, no. 5, pp. 445–452, Oct. 2003.
[11] T. Komine, J. Lee, S. Haruyama, and M. Nakagawa, "Adaptive equalization for indoor visible-light wireless communication systems," in *Proc. Asia-Pac. Conf. Commun.*, 2005, pp. 294–298.
[12] H. Zhu and J. Wang, "Chunk-based resource allocation in OFDMA systems–Part I: Chunk allocation," *IEEE Trans. Commun.*, vol. 57, no. 9, pp. 2734–2744, Sep. 2009.
[13] H. Zhu and J. Wang, "Chunk-based resource allocation in OFDMA systems–Part II: Joint chunk, power and bit allocation," *IEEE Trans. Commun.*, vol. 60, no. 2, pp. 499–509, Feb. 2012.
[14] O. Gonzalez, R. Perez-Jimenez, S. Rodriguez, J. Rabadan, and A. Ayala, "OFDM over indoor wireless optical channel," *Proc. Inst. Elect. Eng.—Optoelectron.*, vol. 152, no. 4, pp. 199–204, Aug. 2005.
[15] J. Armstrong, B. Schmidt, D. Kalra, H. Suraweera, and A. Lowery, "SPC07-4: Performance of asymmetrically clipped optical OFDM in AWGN for an intensity modulated direct detection system," in *Proc. IEEE Global Telecommun. Conf.*, 2006, pp. 1–5.
[16] J. Armstrong, "OFDM for optical communications," *J. Lightwave Technol.*, vol. 27, no. 3, pp. 189–204, Feb. 2009.
[17] B. Popovic, "Spreading sequences for multicarrier CDMA systems," *IEEE Trans. Commun.*, vol. 47, no. 6, pp. 918–926, Jun. 1999.
[18] F. Alsaadi and J. M. H. Elmirghani, "Adaptive mobile line strip multibeam MC-CDMA optical wireless system employing imaging detection in a real indoor environment," *IEEE J. Sel. Areas Commun.*, vol. 27, no. 9, pp. 1663–1675, Dec. 2009.

[19] Y. Zhou, J. Wang, and M. Sawahashi, "Downlink transmission of broadband OFCDM systems—Part I: Hybrid detection," *IEEE Trans. Commun.*, vol. 53, no. 4, pp. 718–729, Apr. 2005.
[20] F. Adachi, M. Sawahashi, and H. Suda, "Wideband DS-CDMA for next-generation mobile communications systems," *IEEE Commun. Mag.*, vol. 36, no. 9, pp. 56–69, Sep. 1998.
[21] V. Jungnickel, V. Pohl, S. Nonnig, and C. Von Helmolt, "A physical model of the wireless infrared communication channel," *IEEE J. Sel. Areas Commun.*, vol. 20, no. 3, pp. 631–640, Apr. 2002.
[22] J. M. Kahn and J. R. Barry, "Wireless infrared communications," *Proc. IEEE*, vol. 85, no. 2, pp. 265–298, Feb. 1997.
[23] K. Fazel and S. Kaiser, *Multi-carrier and spread spectrum systems: From OFDM and MC-CDMA to LTE and WiMAX*. Hoboken, NJ, USA: Wiley, 2008. [Online]. Available: Wiley.com
[24] R. A. Horn and C. R. Johnson, *Matrix Analysis*. Cambridge, U.K.: Cambridge Univ. Press, 2012.
[25] J. G. Proakis, *Digital Communications*. New York, NY, USA: McGraw-Hill, 2001.
[26] B. Sklar, *Digital communications: Fundamentals and Applications*. Englewood Cliffs, NJ, USA: Prentice-Hall, 2001.
[27] Y. Zhou, J. Wang, and T.-S. Ng, "Downlink transmission of broadband OFCDM systems—Part V: Code assignment," *IEEE Trans. Wireless Commun.*, vol. 7, no. 11, pp. 4546–4557, Nov. 2008.
[28] L. Yang and E. Alsusa, "Dynamic code-allocation based PAPR reduction technique for MC-CDMA systems," in *Proc. IEEE Wireless Commun. Netw. Conf.*, 2007, pp. 627–632.